



Renewable hydrogen production from oxidative steam reforming of bio-butanol over CoIr/CeZrO₂ catalysts: Relationship between catalytic behaviour and catalyst structure

Weijie Cai^{a,b,1}, Narcis Homs^{a,b}, Pilar Ramirez de la Piscina^{a,*}

^a Departament de Química Inorgànica and Institut de Nanociència i Nanotecnologia, Universitat de Barcelona, Martí i Franquès 1-11, 08028 Barcelona, Spain

^b Catalonia Institute for Energy Research (IREC), Jardins de les Dones de Negre 1, 08930 Barcelona, Spain

ARTICLE INFO

Article history:

Received 19 July 2013

Received in revised form

18 November 2013

Accepted 20 November 2013

Available online 1 December 2013

Keywords:

Bio-butanol

Oxy-steam reforming

Structure sensitivity

Renewable hydrogen

CeO₂–ZrO₂

ABSTRACT

Several bimetallic CoIr/Ce_{0.82}Zr_{0.18}O₂ catalysts with supports of different characteristics were studied in the oxidative steam reforming of a bio-butanol raw mixture (*n*-butanol/acetone/ethanol = 6/3/1, mass ratio). Ce_{0.82}Zr_{0.18}O₂ supports were prepared by precipitation and then calcination at different temperatures (500 °C, 700 °C and 900 °C). The calcination temperature of the support determined certain characteristics of the final catalyst, namely: BET surface area, crystallite size, basicity, reduction properties and oxygen storage capacity (OSC). All of these factors were found to affect the performance of the catalysts in terms of: raw mixture conversion, hydrogen selectivity and resistance to deactivation upon long-term testing. Several techniques such as XRD, TPR, CO₂ TPD, CO₂ adsorption calorimetry, Raman, DRIFT, TEM, XPS and OSC were used to characterize the catalysts. Characterization of samples before and after catalytic tests allowed us to determine the influence of the catalyst characteristics on the deactivation process.

© 2013 Elsevier B.V. All rights reserved.

1. Introduction

In recent decades, our dependence on fossil energy sources has caused serious environmental problems. The use of hydrogen as an energy carrier could contribute to sustainable energy development if renewable hydrogen production is contemplated. This is the reason why hydrogen production from biomass-derived sources has attracted much attention [1–3]. Bio-butanol can be produced from a sugary biomass by fermentation; a specific mixture (butanol/acetone/ethanol = 6/3/1, mass ratio) is considered a model of the bio-butanol raw mixture obtained [4]. Oxidative steam reforming of bio-butanol is a potential strategy for hydrogen production due to the ease of bio-butanol transport, its renewable character and its high hydrogen content [5,6]. Furthermore, reformation of the preliminary liquid raw mixture (butanol/acetone/ethanol = 6/3/1, mass ratio) is favourable in terms of energy, as no further distillation is necessary.

Although there are few studies concerning bio-butanol reforming processes, other renewable higher alcohols, such as ethanol and

glycerol have been extensively studied over supported metal catalysts, and the influence of the support on the catalytic behaviour of the samples is well recognized [2]. CeO₂–ZrO₂ oxides have been proposed as supports for catalytic reformation of ethanol and glycerol, because of their thermal stability and OSC [7,8]. Insertion of Zr⁴⁺ into the CeO₂ structure leads to structural distortions of the ceria fluorite lattice which improve its OSC, thermal stability and resistance to sintering. Since Zr⁴⁺ is smaller than Ce⁴⁺, it can contribute to removing the strain associated with the increase of size accompanying the Ce⁴⁺ to Ce³⁺ transition, and therefore to enhancing the ceria redox capacity and facilitating oxygen mobility [9]. Computer simulation studies revealed that even small additions of ZrO₂ greatly facilitate bulk Ce⁴⁺ reduction compared to pure CeO₂ [10]. The surface basicity, OSC and metal-support interactions are characteristics of primary importance for catalysts used in reforming processes [11]. For CeO₂–ZrO₂ supports, both their composition and their method of preparation could determine these characteristics and consequently the catalytic behaviour of these catalysts in reforming processes. Ethanol steam reforming has been studied over different M/Ce_{1-x}Zr_xO₂ catalysts. When Rh/Ce_{1-x}Zr_xO₂ (*x* = 0.2, 0.4, 0.6, 0.8) were used as catalysts, Rh/Ce_{0.8}Zr_{0.2}O₂ showed the highest H₂ and CO₂ yield and the lowest deactivation rate due to the formation of carbon deposits [12]. Likewise, a study of ethanol steam reforming over Ni/Ce_{1-x}Zr_xO₂ (*x* = 0, 0.26, 0.59, 0.84, 1) revealed that Ni/Ce_{0.74}Zr_{0.26}O₂ had the highest activity, which

* Corresponding author. Tel.: +34 934037056; fax: +34 934907725.

E-mail address: pilar.piscina@qi.ub.es (P. Ramirez de la Piscina).

¹ Actual address: Faculty of Light Industry and Chemical Engineering, Dalian Polytechnic University, 116023 Dalian, China.

was related to it having the most reduced nickel available for reaction [13]. In fact, the high OSC of cubic $\text{Ce}_{0.74}\text{Zr}_{0.26}\text{O}_2$ can increase the availability of surface oxygen, which can itself contribute to the WGS reaction and increase the H_2 yield in reformation reactions [13].

The better catalytic performance in the auto-thermal reforming of ethanol over $\text{Ni/CeO}_2\text{-ZrO}_2$ samples than over Ni/ZrO_2 has been related to the higher dispersion of nickel species and the higher OSC [7]. However, the segregation of bulk CeO_2 in $\text{Ni/CeO}_2\text{-ZrO}_2$ catalysts with a support composition of $\text{Ce}_{0.48}\text{Zr}_{0.52}\text{O}_2$ was related to poorer catalytic performance due to the less oxygen provided on the catalyst surface [7].

With respect to the metallic phase, the addition of a second metal to a monometallic catalyst can have several beneficial effects on the behaviour of the material in the reforming process; a review of this work was recently published [14]. We studied non-oxidative and oxidative steam reforming of the bio-butanol raw mixture over cobalt-based catalysts. The presence of small amounts of noble metals facilitated the reduction of the cobalt species thereby contributing to the enhanced performance of the catalysts [15–18]. Specifically, we have recently shown that the Rh and Ir addition to Co/ZnO catalysts decreases both the cobalt sintering and the carbon deposits under oxidative steam reforming of the bio-butanol raw mixture (OSRB) [18]. Taking into account our recent results regarding OSRB together with the background of the use of $\text{CeO}_2\text{-ZrO}_2$ -supported catalysts in the reforming of higher alcohols, here we study the oxidative steam reforming of bio-butanol raw mixture (OSRB) over $\text{CoIr/Ce}_{0.82}\text{Zr}_{0.18}\text{O}_2$ catalysts. The aim of this work is to establish the main parameters that influence the behaviour of $\text{CoIr/Ce}_{0.82}\text{Zr}_{0.18}\text{O}_2$ in OSRB for H_2 production. Catalysts were tested in OSRB at initial conversion values lower than 100% and this allowed to follow the deactivation. Different calcination temperatures of the support provided catalysts with a similar composition but different intrinsic characteristics which determine the catalytic behaviour. In order to establish the structure-catalytic behaviour relationship, catalysts were characterized using: temperature-programmed reduction (TPR), X-ray diffraction (XRD), Raman spectroscopy, X-ray photoelectron spectroscopy (XPS), oxygen storage capacity (OSC), CO_2 temperature programmed desorption (TPD), CO_2 adsorption calorimetry, CO chemisorption followed by diffuse reflectance infrared Fourier transform (DRIFT) spectroscopy and transmission electron microscopy (TEM).

2. Experimental

2.1. Catalyst preparation

$\text{Ce}_{0.82}\text{Zr}_{0.18}\text{O}_2$ supports were prepared using urea as the precipitation agent. An aqueous solution containing $\text{Ce}(\text{NO}_3)_3 \cdot 6\text{H}_2\text{O}$, $\text{ZrO}(\text{NO}_3)_2 \cdot x\text{H}_2\text{O}$ and urea was treated at 90°C under stirring for 6 h. After filtration and thorough washing with water, the precipitate was dried at 70°C overnight and finally calcined at 500°C , 700°C or 900°C for 5 h in air, yielding the supports $\text{Ce}_{0.82}\text{Zr}_{0.18}\text{O}_2$ 500, $\text{Ce}_{0.82}\text{Zr}_{0.18}\text{O}_2$ 700 and $\text{Ce}_{0.82}\text{Zr}_{0.18}\text{O}_2$ 900, respectively. Catalysts, containing approximately 7% Co by weight and 0.3% Ir by weight, were prepared by incipient wetness impregnation using an aqueous solution containing $\text{Co}(\text{NO}_3)_2 \cdot 6\text{H}_2\text{O}$ and $\text{IrCl}_3 \cdot x\text{H}_2\text{O}$. The impregnated samples were dried at 70°C overnight and then calcined at 450°C in air for 5 h. The catalysts were thus named: $\text{CoIr/Ce}_{0.82}\text{Zr}_{0.18}\text{O}_2$ 500, $\text{CoIr/Ce}_{0.82}\text{Zr}_{0.18}\text{O}_2$ 700 and $\text{CoIr/Ce}_{0.82}\text{Zr}_{0.18}\text{O}_2$ 900.

2.2. Catalyst characterization

The metal content was analyzed by inductively-coupled plasma atomic emission spectrometry using ICP-OES Perkin Elmer Optima 3200RL equipment.

N_2 adsorption-desorption isotherms were recorded at -196°C using a Micromeritics Tristar-II. Prior to the measurements, the samples were outgassed at 150°C for 2 h. The specific surface area was calculated by multi-point BET analysis of the nitrogen adsorption isotherms.

XRD patterns were recorded using a Siemens D-500 X-ray diffractometer with nickel-filtered $\text{CuK}\alpha_1$ radiation. The XRD profiles were collected between $2\theta = 20^\circ$ and 100° , with a step width of 0.05° counting 3 s at each step. The mean crystallite size of the particles was calculated according to the Debye-Scherrer equation.

H_2 -TPR, OSC and CO_2 -TPD experiments were performed using a Micromeritics AutoChem-II chemisorption analyser. For the H_2 -TPR experiments, about 40 mg of each catalyst was pretreated at 100°C for 1 h under flowing He. After cooling to room temperature, the sample was exposed to a flow of H_2/Ar (12% vol/vol, 50 mL/min), and the temperature was linearly increased at $10^\circ\text{C}/\text{min}$ up to 800°C .

The OSC of the catalysts was measured using the oxygen pulse injection method. Before analysis, the samples (50 mg) were reduced with H_2/Ar (12%, vol/vol, 50 mL/min); the temperature was linearly increased at $10^\circ\text{C}/\text{min}$ up to 800°C and was kept at 800°C during 5 min. Then, they were cooled to 300°C under Ar flow (50 mL/min). A stream of O_2/He (10% vol/vol, 50 mL/min) was periodically injected into the reduced sample until saturation and accordingly the consumption of oxygen was calculated.

Prior to the CO_2 -TPD runs, the catalyst (100 mg) was reduced under flowing H_2/Ar (12% vol/vol, 50 mL/min) for 1 h at 450°C and then cooled to 30°C under flowing He. The adsorption of CO_2 was carried out using a feed of CO_2/Ar (10% vol/vol) for 1 h. The reactor was then purged with He for 30 min. The temperature was increased to 800°C at a rate of $10^\circ\text{C}/\text{min}$, under a He flow.

The CO_2 adsorption was also evaluated by calorimetry. The adsorption enthalpy of CO_2 was measured by differential scanning calorimetry (DSC) using a Sensys evo DSC instrument (Setaram) equipped with a 3D thermal flow sensor. The sample was loaded into twin fixed-bed reactors, with one reactor serving as the reference. The sample was firstly reduced in H_2/Ar (12% vol/vol) for 2 h at 450°C and then cooled down to 30°C under Ar flow. A flowing mixture of CO_2/Ar (10% vol/vol) was admitted to the catalyst at 30°C . The exothermic peak corresponding to CO_2 adsorption was integrated to provide the total enthalpy of adsorption for the amount of CO_2 adsorbed. The mean heat of adsorption per mole of adsorbed CO_2 was determined by considering the total amount of CO_2 adsorbed.

XPS was performed using a VG Escalab 200R spectrometer with $\text{MgK}\alpha$ ($h\nu = 1253.6\text{ eV}$) at a pressure of 4×10^{-9} mbar during data acquisition. The charging effect was corrected by referencing the binding energy of C 1s at 284.9 eV and the spectra were curve-fitted using a Gaussian-Lorentzian procedure.

In situ DRIFT spectroscopy of CO adsorption was recorded using a Nicolet Magna-IR 750 FTIR spectrometer equipped with a liquid nitrogen-cooled MCT detector and a Spectra Tech catalytic chamber. The spectra recorded consisted of 64 scans at 4 cm^{-1} resolution. Prior to CO adsorption, the reduced samples were re-reduced in situ in the catalytic chamber under an H_2/Ar flow (12% vol/vol) at 400°C and then cooled to room temperature under a He flow. Carbon monoxide (10% vol/vol CO/He) was brought into contact with the reduced catalysts at room temperature; the samples were outgassed with He at room temperature; and then their spectra were recorded.

Table 1

Surface area, oxygen storage capacity (OSC), and composition determined by chemical analysis of calcined catalysts.

Catalyst	S_{BET} (m^2/g)	OSC ($\mu\text{molO}/\text{g}_{\text{cat}}$)	Co (wt%)	Ir (wt%)
Colr/Ce _{0.82} Zr _{0.18} 500	72	319	6.46	0.28
Colr/Ce _{0.82} Zr _{0.18} 700	25	152	6.65	0.24
Colr/Ce _{0.82} Zr _{0.18} 900	14	44	6.66	0.27

Raman spectra were recorded using a Jobin-Yvon Lab Ram HR 800 with a solid state laser at 532.1 nm and a CCD detector. The Raman spectra of the catalysts were collected with the laser power limited to 0.7 mW to minimize laser-heating effects.

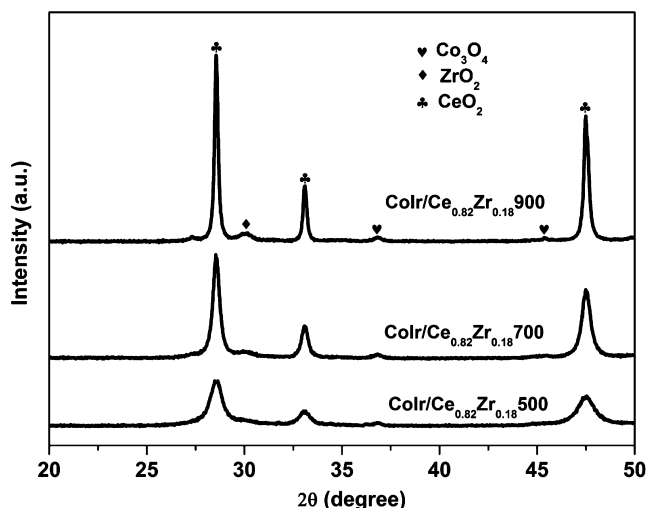
TEM images were obtained using a J1010 microscope. Ethanol suspensions of the samples were prepared by ultrasonic treatment and then they were deposited onto a copper grid to be studied.

2.3. Catalytic measurements

Catalytic reforming tests were carried out in a Microactivity-Reference unit (PID Eng&TECH). The catalysts were mixed with inactive SiC (Prolabo, 0.5 mm) and placed in a tubular fixed-bed reactor (305 mm long, 9 mm i.d., 316-L stainless steel) up to a catalytic volume of approximately 1 mL. The temperature was measured using a thermocouple in direct contact with the catalytic bed. Before the reaction, the catalyst (300 mg) was reduced under an H₂/Ar mixture (H₂/Ar 10% vol/vol) at 450 °C for 1.5 h. Two piston pumps were used to introduce bio-butanol (butanol/acetone/ethanol = 6/3/1, mass ratio) and water separately. The liquid mixture was then vaporized and mixed with a controlled flow of dilution gas (Ar) and air to achieve the desired O₂ concentration in the reactant flow ($S/C = 3$; raw mixture/O₂ = 1/1.5; GHSV = 7500 h⁻¹). The products were analyzed on-line with a Varian 450-GC equipped with a TCD detector, a methanizer and two FID detectors.

3. Results and discussion

As stated in the Experimental section, three Ce_{0.82}Zr_{0.18}O₂ oxides were prepared by precipitation and then calcination at 500 °C, 700 °C and 900 °C and used as supports for Colr catalysts with approximately 7% Co (wt/wt) and 0.3% Ir (wt/wt). Table 1 shows several characteristics of the calcined catalysts. Their BET surface areas declined with the increasing calcination temperature of the support: a decrease from 72 m²/g (Colr/Ce_{0.82}Zr_{0.18}500) to 25 m²/g (Colr/Ce_{0.82}Zr_{0.18}700) and 14 m²/g (Colr/Ce_{0.82}Zr_{0.18}900).

**Fig. 1.** XRD patterns of calcined catalysts.**Table 2**

Crystallite sizes calculated from the XRD patterns.

Catalyst	Co ₃ O ₄ d (nm)		CeO ₂ d (nm)		t-ZrO ₂ d (nm)	
	Calcined		Calcined	Used	Calcined	Used
Colr/Ce _{0.82} Zr _{0.18} 500	11		11	13	–	–
Colr/Ce _{0.82} Zr _{0.18} 700	12		17	18	9	11
Colr/Ce _{0.82} Zr _{0.18} 900	14		36	38	10	12

In all cases, the XRD patterns of the calcined catalysts (Fig. 1) exhibited diffraction peaks that were assigned to the support and to the presence of Co₃O₄ particles; no diffraction lines that could have been considered characteristics of Ir-containing phases were present. All the XRD patterns were dominated by the presence of peaks characteristic of CeO₂ with a fluorite structure (JCPDS 00-034-0394). Moreover, the XRD patterns of Colr/Ce_{0.82}Zr_{0.18}700 and Colr/Ce_{0.82}Zr_{0.18}900 showed a peak at $2\theta = 29.9^\circ$ which corresponded to the more intense peak of tetragonal ZrO₂ (JCPDS 01-088-1007); this indicates that the segregation of t-ZrO₂ crystallites takes place at a calcination temperature of 700 °C or higher. From the XRD pattern of Colr/Ce_{0.82}Zr_{0.18}500, the formation of a Ce_{1-x}Zr_xO₂ cubic solid solution is envisaged; since a slight displacement of the position of the peaks characteristic of CeO₂ to higher 2θ angle values is noted ((1 1 1) diffraction peak from 28.54° in Colr/Ce_{0.82}Zr_{0.18}900 to 28.58° in Colr/Ce_{0.82}Zr_{0.18}500). The crystallite size of CeO₂ were calculated for all catalysts from the (1 1 1) peak, using the Debye–Scherrer equation. The size, which was in the range 11–36 nm, increased significantly with increasing calcination temperature of the support (Table 2). For Colr/Ce_{0.82}Zr_{0.18}500, in which no segregation of crystalline ZrO₂ existed, the external surface obtained from XRD (77 m²/g) was close to the BET surface area (72 m²/g); at least in this catalyst the presence of mainly monocrystalline Ce_{1-x}Zr_xO₂ grains is thus deduced. A crystallite size of 9 nm and 10 nm was calculated for t-ZrO₂ in Colr/Ce_{0.82}Zr_{0.18}700 and Colr/Ce_{0.82}Zr_{0.18}900, respectively; for this calculation, the (1 0 1) peak, which is the most intense of t-ZrO₂, was used. The crystallite size of Co₃O₄ particles determined by XRD increased slightly when the calcination temperature of the support was increased from 500 °C to 900 °C; the crystallite size calculated from the (3 1 1) peak of the Co₃O₄ phase was in the 11–14 nm range. This small increase in the crystallite size of Co₃O₄ is consistent with that which was observed in CeO₂, as mentioned above (11–36 nm).

Fig. 2 shows the TPR profiles of the catalysts and those of the corresponding supports. Two broad peaks centered at 450–475 °C and

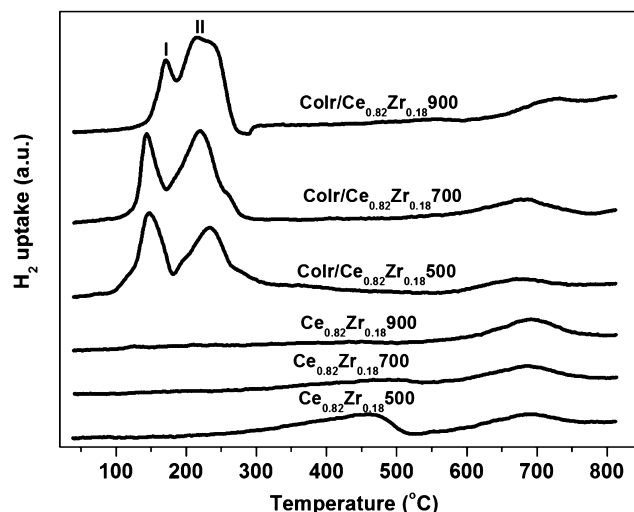
**Fig. 2.** H₂-TPR profiles of supports and catalysts.

Table 3
Hydrogen consumption during TPR experiments compared to theoretical consumption.

Catalyst	H ₂ consumption (μmol H ₂ /g _{cat})				
	Experimental peaks I and II	Theoretical total	Experimental peak I	Theoretical IrO ₂ reduction	Theoretical Co ₃ O ₄ to CoO reduction
CoIr/Ce _{0.82} Zr _{0.18} 500	2179	1489	806	29	365
CoIr/Ce _{0.82} Zr _{0.18} 700	1964	1528	565	25	381
CoIr/Ce _{0.82} Zr _{0.18} 900	1804	1533	446	28	376

690 °C were clearly visible for Ce_{0.82}Zr_{0.18}500 and Ce_{0.82}Zr_{0.18}700 supports; the peak located at 450–475 °C which intensity decreased with the increase of calcination temperature of the support, is related with the reduction of Ce⁴⁺ surface species. The TPR profiles of the three catalysts showed two main peaks of H₂ consumption (peaks I and II); the minor contribution at about 700 °C is related with the support reduction. The catalysts showed significant differences in both the TPR profile and the amount of H₂ consumed (Table 3). The peak at the lower temperature (peak I) showed the maximum of H₂ consumption at 144 °C in the profile of CoIr/Ce_{0.82}Zr_{0.18}500 and CoIr/Ce_{0.82}Zr_{0.18}700, and at 162 °C in the profile corresponding to CoIr/Ce_{0.82}Zr_{0.18}900. Moreover, peak I corresponding to CoIr/CeZr500 was wider than for the other two catalysts and showed a shoulder at approximately 125 °C. The amount of hydrogen consumed corresponding to peak I calculated by deconvolution appears in Table 3. As a reference, Table 3 also shows the theoretical H₂ consumption necessary for the reduction of IrO₂ to Ir and that necessary for the reduction of Co₃O₄ to CoO, which is the first step in Co₃O₄ reduction. In all the cases, the amount of H₂ corresponding to peak I largely exceeded that required for the reduction of IrO₂ to Ir; this excess of H₂ is related to the reduction of Co₃O₄ particles in CoIr/Ce_{0.82}Zr_{0.18}O₂ which are favoured, via hydrogen spillover, by the presence of Ir. This may be related to close contact between the cobalt and iridium species, as has already been proposed to occur in other Co-noble metal catalysts [19,20]. Moreover, a contribution to peak I of the reduction of Ce⁴⁺ species cannot be ruled out; recently the reduction of Ce⁴⁺ species at a temperature lower than 150 °C was reported for Ir/CeO₂ catalysts [21]. The amount of H₂ consumption corresponding to the peak I exceeds by 104% (CoIr/Ce_{0.82}Zr_{0.18}500), 39% (CoIr/Ce_{0.82}Zr_{0.18}700) and 11% (CoIr/Ce_{0.82}Zr_{0.18}900) that necessary to reduce IrO₂ to Ir and Co₃O₄ to CoO. The extension of the reduction of cobalt species (and/or Ce⁴⁺ species) achieved at a low temperature (peak I) increases when the calcination temperature of the support decreases. Table 3 also compares the hydrogen consumed (peaks I and II) in the TPR experiments and the theoretical consumption of H₂, assuming reduction of Co₃O₄ and IrO₂ to Co and Ir, respectively. In all the cases, the experimental value (peaks I and II) was higher than the theoretical one and the amount of excess hydrogen consumed was in the order: CoIr/Ce_{0.82}Zr_{0.18}500 (46%) > CoIr/Ce_{0.82}Zr_{0.18}700 (29%) > CoIr/Ce_{0.82}Zr_{0.18}900 (18%). Peaks II are related with the reduction of the remaining cobalt oxides and the partial reduction of Ce⁴⁺ species to Ce³⁺. As stated in the Introduction section, the addition of Zr⁴⁺ to ceria enhances the ceria redox capacity and facilitates bulk Ce⁴⁺ reduction [10]. Moreover, in our case, the presence of Co and Ir phases should significantly contribute to enhancing the degree of Ce⁴⁺ reduction; probably due to hydrogen spillover. The extent of the reduction of Ce⁴⁺ species was higher when the calcination temperature of the support was lower; a lower calcination temperature produces smaller crystallites of Ce_{1-x}Zr_xO₂ or CeO₂ and Co₃O₄ phases in the catalyst. Furthermore, less Ce_{1-x}Zr_xO₂ may be present when the calcination temperature of the support was increased, as deduced from the XRD characterization; as stated above, the presence of Ce_{1-x}Zr_xO₂ may produce an increase of the reducibility of the support with respect to CeO₂. A change in the

nature of the metal–support interaction and/or the number of interface sites with the change in the calcination temperature of the support is suggested [11].

The catalysts were compared in terms of their OSC because this parameter may be related to the different reducibility of catalysts and with their catalytic behaviour in the OSRB. To this end, the catalysts were reduced up to 800 °C and then the uptake of O₂ at 300 °C was determined. To evaluate the effective amount of OSC related to the support, total values of O₂ uptake were corrected according the Co and Ir redox contributions (oxidation to Co₃O₄ and IrO₂); results are reported in Table 1. The OSC values showed a marked decrease in the O₂ storage capacity when the calcination temperature of the support increased; OSC values varied from 319 μmolO/g_{cat} for CoIr/Ce_{0.82}Zr_{0.18}500 to 44 μmolO/g_{cat} for CoIr/Ce_{0.82}Zr_{0.18}900. The decrease of the OSC of the catalysts when the calcination temperature of the support increased is related to the decrease in oxygen mobility, the lower reducibility of the catalysts and probably the simultaneous decrease in the defect density in Ce_{1-x}Zr_xO₂ or CeO₂; using XRD, it was shown that an increase of calcination temperature produced an increase in the crystallite size of CeO₂ (or Ce_{1-x}Zr_xO₂) and the segregation of *t*-ZrO₂. Although the surface area of the catalysts decreased when the calcination temperature of the support increased, it was shown previously that for Ce_{1-x}Zr_xO₂ solids, OSC is directly correlated with the concentration of vacancy-interstitial oxygen defects, while the surface area exhibited much less of a correlation [22].

The XRD patterns of the reduced catalysts do not allow for identification of phases other than those corresponding to the support. After reduction, the XRD patterns did not show diffraction peaks characteristic of Co₃O₄ or those corresponding to reduced phases containing cobalt. It was expected that the reduction treatment would produce metallic Co particles. The most intense XRD peak corresponding to Co_{fcc} (JCPDS 00-015-0806) is located at 2θ = 44.2°; while that corresponding to Co_{hcp} (JCPDS 01-089-4308) is at 2θ = 47.4°. This latter peak would overlap with the (2 2 0) peak

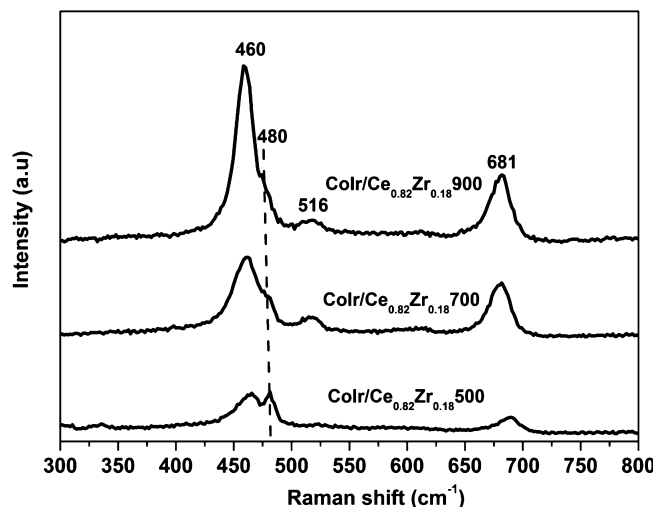


Fig. 3. Raman spectra of reduced catalysts.

of cubic CeO_2 (or $\text{Ce}_{1-x}\text{Zr}_x\text{O}_2$). The low Ir content may account for the absence of peaks characteristic of Ir-containing phases.

Raman spectra for the reduced catalysts are shown in Fig. 3. The band at approximately $460\text{--}465\text{ cm}^{-1}$ was assigned to the F_{2g} vibration of the fluorite-type lattice ($\text{Ce}_{1-x}\text{Zr}_x\text{O}_2$ or CeO_2). It can be viewed as a symmetric breathing mode of the oxide ions around the cerium ions [23]. The intensity and shape of the F_{2g} band changed with the calcination temperature of the support; the intensity of the band was greater and it was located at a lower Raman shift as the calcination temperature was increased. The increase in the intensity of the F_{2g} band is related to better crystallization of the cubic $\text{Ce}_{1-x}\text{Zr}_x\text{O}_2$ or CeO_2 when the calcination temperature was increased, in accordance with the XRD results. Although for CeO_2 nanocrystals a decrease in the Raman shift of the F_{2g} band referred to bulk CeO_2 has been reported [23], the slight decrease in the Raman shift of the F_{2g} band from $\text{CoIr/Ce}_{0.82}\text{Zr}_{0.18}500$ (465 cm^{-1}) to $\text{CoIr/Ce}_{0.82}\text{Zr}_{0.18}900$ (460 cm^{-1}) may be related to the different composition of $\text{Ce}_{1-x}\text{Zr}_x\text{O}_2$ in the catalysts [24,25]; the XRD results showed the partial segregation of tetragonal ZrO_2 in $\text{CoIr/Ce}_{0.82}\text{Zr}_{0.18}700$ and $\text{CoIr/Ce}_{0.82}\text{Zr}_{0.18}900$ from the $\text{Ce}_{1-x}\text{Zr}_x\text{O}_2$ solid solution. However, there was no evidence in any case of the formation of $t\text{-ZrO}_2$ in the Raman spectra, since $t\text{-ZrO}_2$ shows six active Raman bands ($\text{A}_{1g} + 3\text{E}_g + 2\text{B}_{1g}$) at 190 cm^{-1} , 270 cm^{-1} , 315 cm^{-1} , 455 cm^{-1} , 602 cm^{-1} and 645 cm^{-1} [26]. The other three bands centered at 480 cm^{-1} , 516 cm^{-1} and 681 cm^{-1} , in the Raman spectra in Fig. 3 were attributed to surface cobalt oxides [27–29], which probably formed due to the ex-situ experimental set-up used to register the Raman spectra.

The surface basicity of reduced catalysts was determined by CO_2 -TPD and by CO_2 adsorption followed by calorimetry. Fig. 4A shows CO_2 -TPD profiles of the catalysts. Large differences were found between the CO_2 -TPD profile of $\text{CoIr/Ce}_{0.82}\text{Zr}_{0.18}500$ and those of the other two catalysts whose supports were calcined at higher temperatures ($\text{CoIr/Ce}_{0.82}\text{Zr}_{0.18}700$ and $\text{CoIr/Ce}_{0.82}\text{Zr}_{0.18}900$). In the CO_2 -TPD profile of $\text{CoIr/Ce}_{0.82}\text{Zr}_{0.18}500$, three main CO_2 desorption zones can be identified: the low temperature zone at $30\text{--}200\text{ }^\circ\text{C}$ (LT), the medium temperature zone at $200\text{--}400\text{ }^\circ\text{C}$ (MT), and the high temperature zone (HT) with CO_2 desorption peaks at temperatures higher than $400\text{ }^\circ\text{C}$. These desorption zones are related to the strength of basic sites on which CO_2 is chemisorbed. The LT peaks are related to the formation of hydrogencarbonates that result from the interaction of CO_2 with weak basicity hydroxyl groups on the surface of the support [30]. The MT peaks correspond to the formation of bridged and bidentate carbonates, and they are associated with the presence of $\text{M}^x\cdots\text{O}^{2-}$ pairs of intermediate basic strength. The HT peaks can tentatively be assigned to the formation of relatively stable carbonates resulting from the reaction of low coordination O^{2-} ions with CO_2 [30]. The amount of desorbed CO_2 from $\text{CoIr/Ce}_{0.82}\text{Zr}_{0.18}700$ and $\text{CoIr/Ce}_{0.82}\text{Zr}_{0.18}900$ at MT and HT was lower than that desorbed from $\text{CoIr/CeZr}500$ (Fig. 4A).

CO_2 adsorption was also followed by calorimetry. Table 4 shows the total number of basic sites per gram of catalyst and the surface density of basic sites (number of basic sites per unit surface area) determined by this technique. Both values decreased with increasing calcination temperature of the support (from $500\text{ }^\circ\text{C}$ to $900\text{ }^\circ\text{C}$). On $\text{CoIr/Ce}_{0.82}\text{Zr}_{0.18}500$, the total number of basic sites per gram of catalyst was almost ten times higher than that on $\text{CoIr/Ce}_{0.82}\text{Zr}_{0.18}900$; and the surface density of basic sites was over twice that of $\text{CoIr/Ce}_{0.82}\text{Zr}_{0.18}900$. The surface density of basic sites decreased almost linearly with the increase of CeO_2 (or $\text{Ce}_{1-x}\text{Zr}_x\text{O}_2$) crystallite sizes as shown in Fig. 4B. Table 4 also shows the mean heat of CO_2 adsorption per gram of catalyst and per mmol of adsorbed CO_2 . Both these CO_2 adsorption heat values decreased when the calcination temperature of the support was increased.

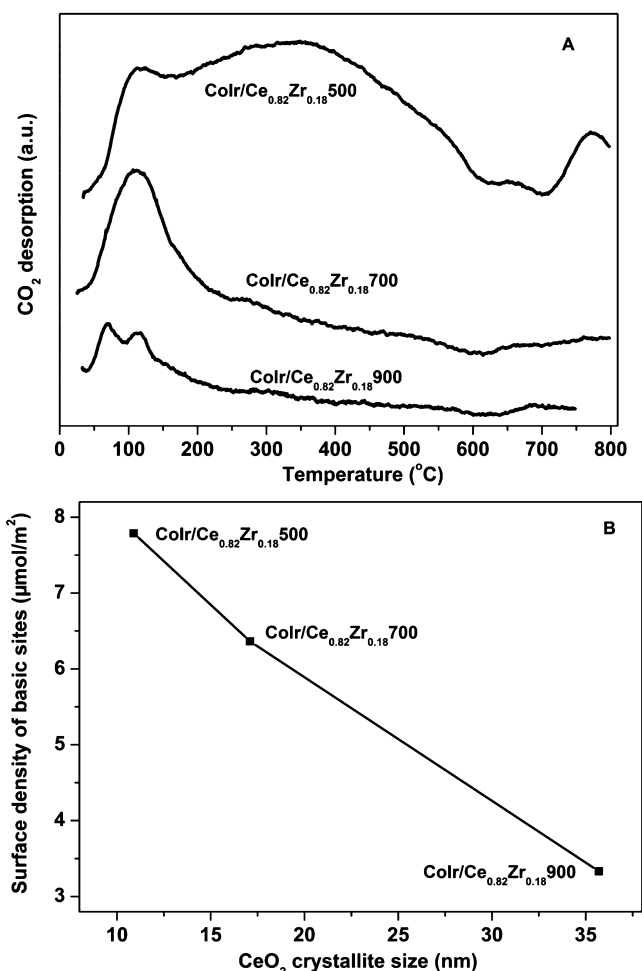


Fig. 4. CO_2 -TPD profiles of reduced catalysts (A) and surface density of basic sites determined by calorimetry as a function of CeO_2 (or $\text{Ce}_{1-x}\text{Zr}_x\text{O}_2$) crystallite size (B).

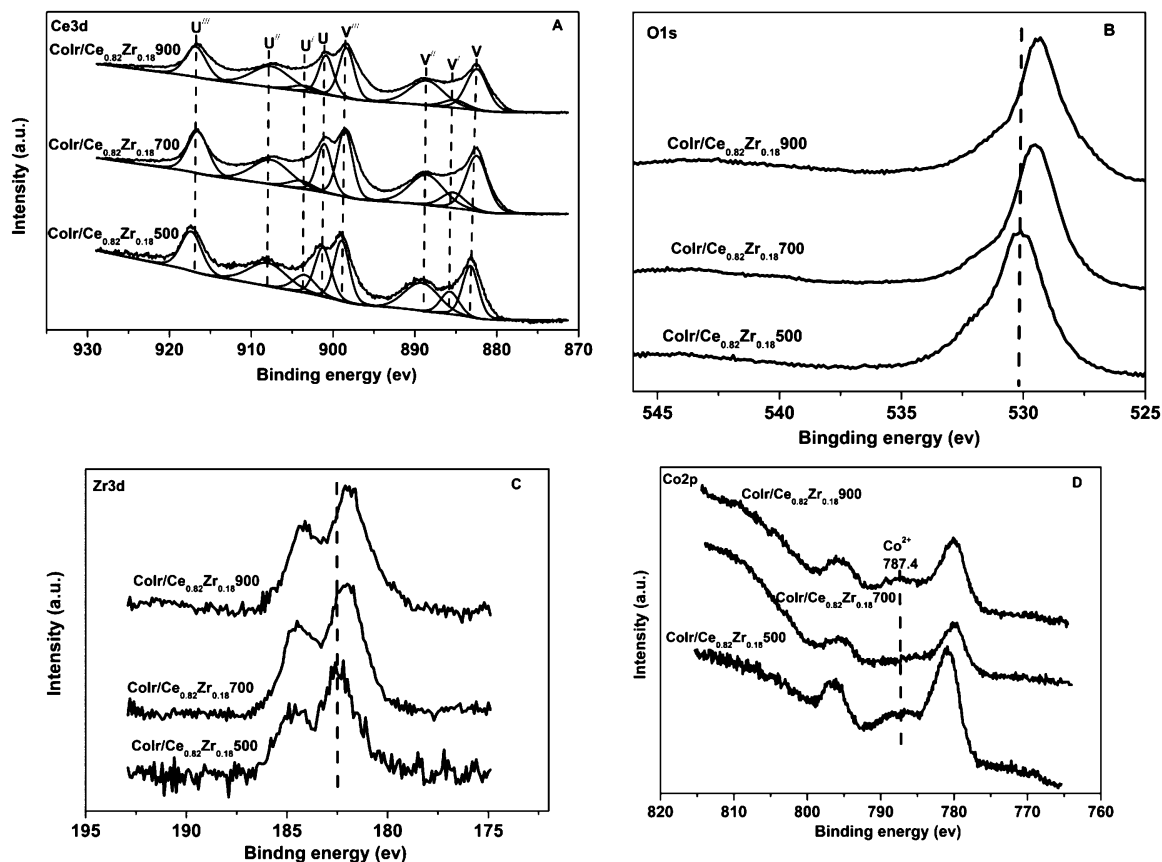
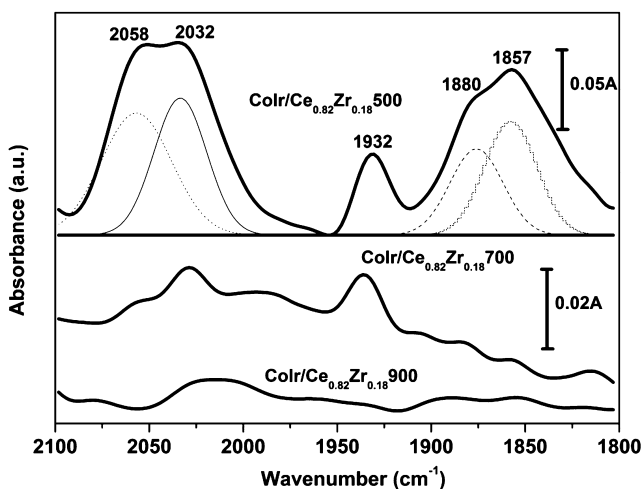
This trend revealed that the mean basic strength per adsorption site declined with increasing support calcination temperature, in accordance with the CO_2 -TPD results. Besides the gradual support sintering, the increase in calcination temperature from $500\text{ }^\circ\text{C}$ to $700\text{ }^\circ\text{C}$ and $900\text{ }^\circ\text{C}$ produced a decrease in the total number of basic sites and the almost total disappearance of basic sites with moderate and strong strength.

The reduced catalysts were also analyzed by XPS; Ce 3d, O 1s, Zr 3d, and Co 2p core level spectra were recorded for all the samples and are shown in Figs. 5A–D, respectively. Due to the overlapping of the Co 3p and Ir 4f levels, surface Ir was not determined by XPS. XPS Ce 3d profiles are usually fitted to eight components, four of them correspond to the Ce $3d_{5/2}$ level (v components) and the other four to the Ce $3d_{3/2}$ level (u components) [9]. Despite the large number of components that can be found when Ce^{3+} and Ce^{4+} are present, v' and u''' can be related to the presence of Ce^{3+} and Ce^{4+} , respectively [9]. The XP spectra of all the catalysts showed both v' and u''' components, which indicates that both Ce^{3+} and Ce^{4+} are present (Fig. 5A). In an attempt to estimate the abundance of Ce^{3+} species in the catalysts, the ratio (v' area/total Ce 3d area) was calculated; the sequence of values of the ratio was $\text{CoIr/Ce}_{0.82}\text{Zr}_{0.18}500 > \text{CoIr/Ce}_{0.82}\text{Zr}_{0.18}700 > \text{CoIr/Ce}_{0.82}\text{Zr}_{0.18}900$ which is in accordance with the trend of the degree of support reduction determined by TPR.

Several differences exist in the XP spectrum of the O 1s core level (Fig. 5B) as a function of the calcination temperature of the

Table 4Calorimetry experiments of CO₂ adsorption at 30 °C; adsorption enthalpy, total basic site concentration and surface density of basic sites.

Catalyst	Heat (J/g _{cat})	Heat (J/mmol CO ₂)	Total basic sites (μmol/g _{cat})	Surface density of basic sites (μmol/m ²)
CoIr/Ce _{0.82} Zr _{0.18} 500	13.5	24.0	560	7.8
CoIr/Ce _{0.82} Zr _{0.18} 700	2.2	13.6	161	6.4
CoIr/Ce _{0.82} Zr _{0.18} 900	0.3	6.5	48	3.3

**Fig. 5.** XPS spectra of reduced catalysts: (A) Ce 3d level; (B) O 1s level; (C) Zr 3d level and (D) Co 2p level.**Fig. 6.** In situ DRIFT spectra of reduced catalysts after CO chemisorption and He flushing at room temperature.

support. Although in all cases the spectrum can be deconvoluted into two components, the catalysts differ in the relative abundance of the components and in the corresponding binding energy (BE) value. The O 1s component at a higher BE has been associated with the presence of surface OH related to adsorbed oxygen [31]. The contribution of this component to the total O 1s spectrum was: 15%, 7% and 6% for CoIr/Ce_{0.82}Zr_{0.18}500, CoIr/Ce_{0.82}Zr_{0.18}700 and CoIr/Ce_{0.82}Zr_{0.18}900, respectively (Fig. 5B). The slightly higher O 1s BE value for CoIr/Ce_{0.82}Zr_{0.18}500 than those corresponding to CoIr/Ce_{0.82}Zr_{0.18}700 and CoIr/Ce_{0.82}Zr_{0.18}900 (see Fig. 5B), would be related to the enrichment of Zr⁴⁺ in the CeO₂ cubic lattice in the first compared to the other two [9]. The Zr 3d spectra also showed differences between the catalysts (Fig. 5C); the shift toward higher BE values of Zr 3d corresponding to CoIr/Ce_{0.82}Zr_{0.18}500 with respect

Table 5

Surface atomic ratios of reduced catalysts determined by XPS compared with atomic ratios determined by chemical analysis (CA).

Catalyst	Co/(Ce + Zr) _{XPS}	Co/(Ce + Zr) _{CA}	Ce/Zr _{XPS}	Ce/Zr _{CA}
CoIr/Ce _{0.82} Zr _{0.18} 500	0.359	0.099	8.369	7.159
CoIr/Ce _{0.82} Zr _{0.18} 700	0.261	0.110	7.208	6.505
CoIr/Ce _{0.82} Zr _{0.18} 900	0.189	0.111	5.113	7.110

to those of $\text{CoIr}/\text{Ce}_{0.82}\text{Zr}_{0.18}700$ and $\text{CoIr}/\text{Ce}_{0.82}\text{Zr}_{0.18}900$ would also pointed the enrichment of Zr^{4+} in the CeO_2 cubic lattice in $\text{CoIr}/\text{CeZr}500$ [9]. All these data are in accordance with the XRD data shown before, which indicate the tetragonal ZrO_2 segregation in $\text{CoIr}/\text{Ce}_{0.82}\text{Zr}_{0.18}700$ and $\text{CoIr}/\text{Ce}_{0.82}\text{Zr}_{0.18}900$ and the formation of a $\text{Ce}_{1-x}\text{Zr}_x\text{O}_2$ cubic phase based on CeO_2 in $\text{CoIr}/\text{Ce}_{0.82}\text{Zr}_{0.18}500$. The Co 2p spectra of the catalysts appear in Fig. 5D. The bands with maxima at 780–781 eV and 795–796 eV correspond to Co 2p_{3/2} and Co 2p_{1/2}, respectively; the width of the bands indicates the coexistence of both Co^0 and oxidized cobalt species on the surface, while the latter were probably formed by oxidation of Co^0 due to air contact before the XP spectra were registered. The band centered at 787.4 eV which is a satellite peak characteristic of the Co^{2+} presence, is more intense in the $\text{CoIr}/\text{Ce}_{0.82}\text{Zr}_{0.18}500$ spectrum than in those of $\text{CoIr}/\text{Ce}_{0.82}\text{Zr}_{0.18}700$ and $\text{CoIr}/\text{Ce}_{0.82}\text{Zr}_{0.18}900$. In Table 5,

the surface Co/Ce + Zr and Ce/Zr atomic ratios of the reduced catalysts as determined by XPS are compared with those determined by chemical analysis. As shown in Table 5, for all the catalysts, the $\text{Co}/(\text{Ce} + \text{Zr})_{\text{XPS}}$ values were higher than the ratios determined by chemical analysis. Moreover, $\text{Co}/(\text{Ce} + \text{Zr})_{\text{XPS}}$ decreased with increasing calcination temperature of the support. In contrast, $\text{Ce}/\text{Zr}_{\text{XPS}}$ was slightly higher than $\text{Ce}/\text{Zr}_{\text{CA}}$ for $\text{CoIr}/\text{Ce}_{0.82}\text{Zr}_{0.18}500$ and $\text{CoIr}/\text{Ce}_{0.82}\text{Zr}_{0.18}700$ but lower for $\text{CoIr}/\text{Ce}_{0.82}\text{Zr}_{0.18}900$; this may be related to the gradual segregation of $t\text{-ZrO}_2$ as the calcination temperature of the support was increased.

The reduced catalysts were also characterized by DRIFT using CO as the probe molecule; this method is said to be very useful for determining the characteristics of the surface metallic centers of bimetallic Co-based catalysts containing noble metals [16,18]. Fig. 6 shows the spectra corresponding to CO adsorption over the

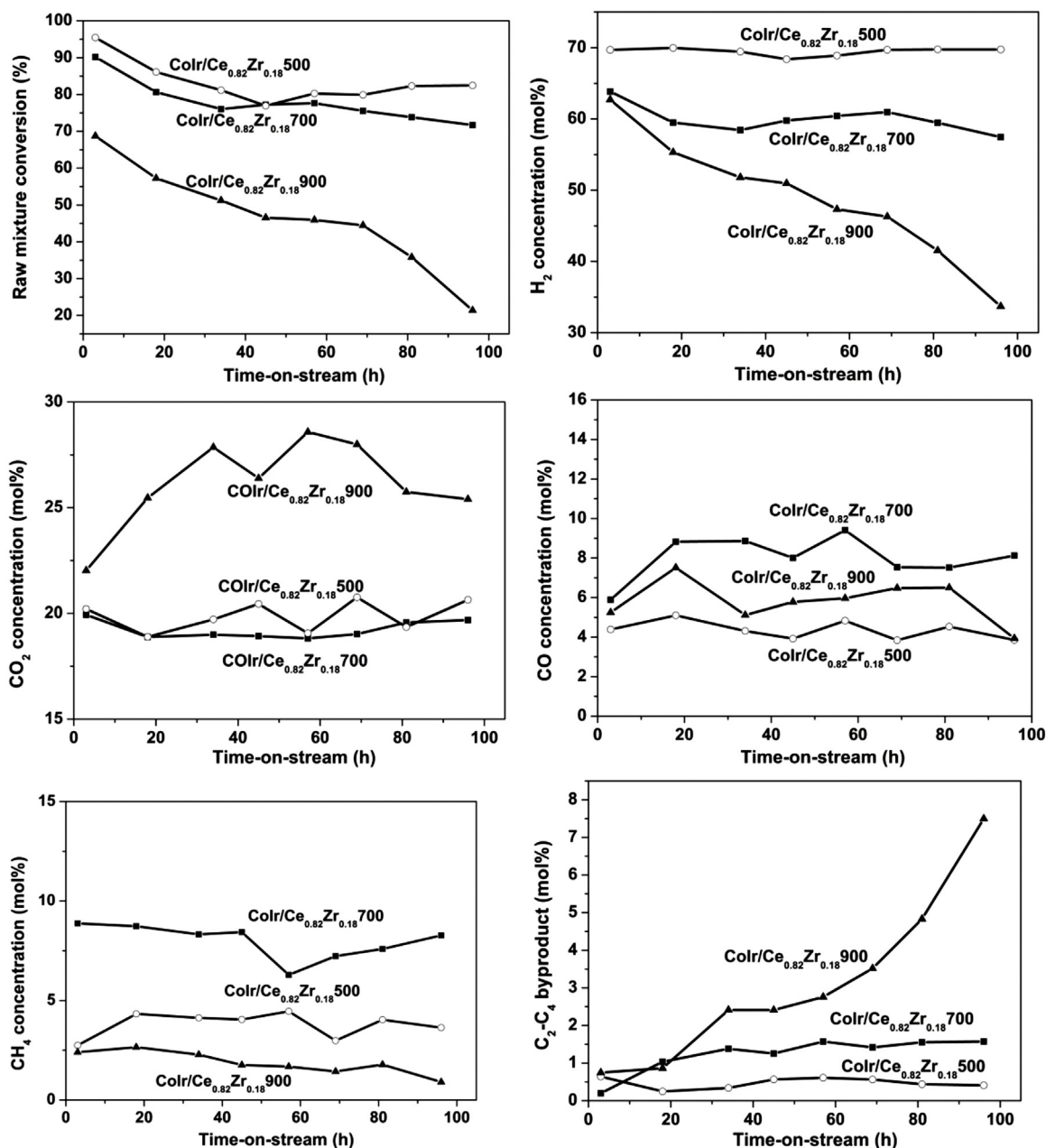


Fig. 7. Catalytic behavior in OSRB. Reaction conditions: $T = 500^\circ\text{C}$; $S/C = 3$; raw mixture/ $\text{O}_2 = 1/1.5$, molar ratio; $n\text{-butanol}/\text{acetone}/\text{ethanol} = 6/3/1$, mass ratio; 300 mg catalyst; $\text{GHSV} = 7500\text{ h}^{-1}$. ($\text{C}_2\text{--C}_4$ by-products: ethylene and butanal).

catalysts. The intensity of the $\nu(\text{CO})$ bands followed the trend: $\text{CoIr}/\text{Ce}_{0.82}\text{Zr}_{0.18}500 > \text{CoIr}/\text{Ce}_{0.82}\text{Zr}_{0.18}700 > \text{CoIr}/\text{Ce}_{0.82}\text{Zr}_{0.18}900$. Although it is difficult to extract quantitative information from DRIFT experiments, comparison of the intensity of the spectra in Fig. 6 indicates that the number of surface metallic centers on $\text{CoIr}/\text{Ce}_{0.82}\text{Zr}_{0.18}500$ is much higher than that on $\text{CoIr}/\text{Ce}_{0.82}\text{Zr}_{0.18}700$ and $\text{CoIr}/\text{Ce}_{0.82}\text{Zr}_{0.18}900$; which is in accordance with the XPS results.

After CO adsorption over $\text{CoIr}/\text{Ce}_{0.82}\text{Zr}_{0.18}500$, three main absorptions in the $\nu(\text{CO})$ zones $2100\text{--}2000\text{ cm}^{-1}$, $1950\text{--}1910\text{ cm}^{-1}$ and $1900\text{--}1800\text{ cm}^{-1}$ were observed; no bands above 2100 cm^{-1} which could be related with the presence of oxidized cobalt species were found. The most intense absorption can be deconvoluted into two bands with maxima at 2058 and 2032 cm^{-1} . The band at 2058 cm^{-1} can reasonably be assigned to CO adsorbed on Co, which interacts with a neighbouring cobalt atom producing a tilt of the CO group; but a contribution to this band of CO adsorbed on Ir cannot be ruled out [16]. Although the band at 2032 cm^{-1} can be related to the presence of linear CO perpendicularly adsorbed to Co^0 , a contribution to this band of CO adsorbed to Ir atoms in small clusters interacting with the support cannot be ruled out [16]. The bands in the $1950\text{--}1800\text{ cm}^{-1}$ region are usually assigned to bridge CO [32]. However, the simultaneous presence of bands at 1930 , $1857\text{--}1880$ and 2032 cm^{-1} may also indicate the presence of $[\text{Co}(\text{CO})_4]^-$ species formed by disproportionation of cobalt carbonyl species coming from the adsorption of CO on very small cobalt entities [33].

Fig. 7 presents the OSRB behaviour of the catalysts at 500°C over a period of approximately 100 h on-stream. The initial raw mixture conversion followed the trend: $\text{CoIr}/\text{Ce}_{0.82}\text{Zr}_{0.18}500$ (95%) $>$ $\text{CoIr}/\text{Ce}_{0.82}\text{Zr}_{0.18}700$ (90%) $>$ $\text{CoIr}/\text{Ce}_{0.82}\text{Zr}_{0.18}900$ (70%). As mentioned above, a similar trend for the density of basic sites determined by CO_2 adsorption and for the ratio $(\text{Co}/\text{Ce} + \text{Zr})_{\text{XPS}}$ was found; the number of metal-support interfacial sites should change similarly. Although there are no mechanistic studies of OSRB, studies of oxidative steam reforming of ethanol over Ir/CeO_2 catalysts indicate the participation of several active sites: ceria surface oxygen vacancies associated with basic hydroxyl groups; metal-support interfacial sites; and Ir surface atoms [11]. In our case, the most sintered catalyst, $\text{CoIr}/\text{Ce}_{0.82}\text{Zr}_{0.18}900$, showed the poorest catalytic performance; probably due to the highest sintering of the metallic phase, and the lowest basicity and redox capacity of the support.

Fig. 7 also shows the evolution of the concentration of the main products in the outlet gas, for all the catalysts. Although in all cases acetone was virtually the only reactant present in the outlet gas, from this work it was not possible to discern whether the acetone in the outlet gas was unconverted reactant or formed by ethanol dehydrogenation and then aldol condensation [34].

The distribution of products was quite stable for $\text{CoIr}/\text{Ce}_{0.82}\text{Zr}_{0.18}500$; this catalyst showed the highest H_2 concentration in the outlet gas (approximately 70 mol%). In contrast, $\text{CoIr}/\text{Ce}_{0.82}\text{Zr}_{0.18}900$ showed a considerable change in the composition of the outlet gas over time: the H_2 concentration decreased greatly (from 63 mol% to 34 mol%) and that of undesirable $\text{C}_2\text{--C}_4$ by-products (mainly ethylene and butanal) increased through time; while raw mixture conversion decreased sharply from 70% to 20%.

After 100 h of reaction, catalyst deactivation followed the order: $\text{CoIr}/\text{Ce}_{0.82}\text{Zr}_{0.18}900$ (68%) $>$ $\text{CoIr}/\text{Ce}_{0.82}\text{Zr}_{0.18}700$ (20%) $>$ $\text{CoIr}/\text{Ce}_{0.82}\text{Zr}_{0.18}500$ (16%).

Carbon formation and the sintering of metal particles have been recognized as major causes of catalyst deactivation in alcohol reforming processes. Moreover, both parameters are strongly influenced by the nature of the support [11,35]. The

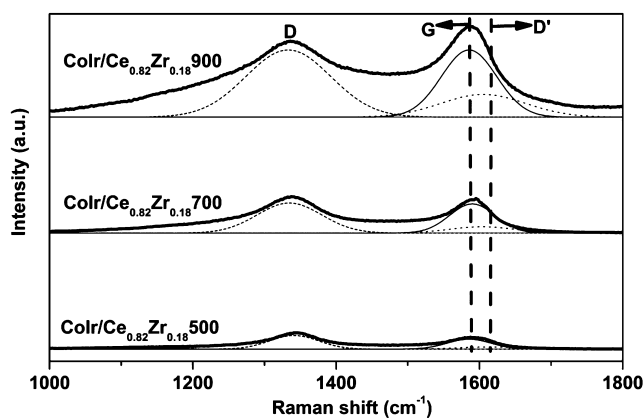


Fig. 8. Raman spectra of post-reaction catalysts.

post-reaction catalysts were characterized by TEM, XRD, and Raman spectroscopy. The XRD patterns of the post-reaction catalysts were similar to those of the reduced catalysts and contained only peaks characteristic of the support. In all cases, the estimated CeO_2 crystallite size of the post-reaction catalysts was only slightly higher than that of the calcined catalyst (Table 2).

The carbonaceous deposits generated during the catalytic tests were characterized by Raman spectroscopy, as this technique allows their degree of order to be estimated [36,37]. Fig. 8 shows the Raman spectra of catalysts in the $1000\text{--}1800\text{ cm}^{-1}$ zone. In all cases, two characteristic bands centered at approximately 1340 cm^{-1} (D band) and $1590\text{--}1600\text{ cm}^{-1}$ appeared. The D band is characteristic of poorly structured carbonaceous deposits; while the band centered at $1590\text{--}1600\text{ cm}^{-1}$ can be deconvoluted into two components: the component at $1575\text{--}1600\text{ cm}^{-1}$ is assigned to the in-plane sp^2 C–C stretching vibrations of well-structured carbon deposits (G' component) and the component at the higher Raman shift ($1600\text{--}1620\text{ cm}^{-1}$, D' component) is associated with less ordered deposits [36,37].

The intensity of the bands which can be related to the amount of carbonaceous deposits formed, followed the trend: $\text{CoIr}/\text{Ce}_{0.82}\text{Zr}_{0.18}900 > \text{CoIr}/\text{Ce}_{0.82}\text{Zr}_{0.18}700 > \text{CoIr}/\text{Ce}_{0.82}\text{Zr}_{0.18}500$. A similar trend was found for the I_G/I_D ratio: $\text{CoIr}/\text{Ce}_{0.82}\text{Zr}_{0.18}900$, $I_G/I_D = 0.61 > \text{CoIr}/\text{Ce}_{0.82}\text{Zr}_{0.18}700$, $I_G/I_D = 0.54 > \text{CoIr}/\text{Ce}_{0.82}\text{Zr}_{0.18}500$, $I_G/I_D = 0.50$. A higher I_G/I_D ratio is related to the presence of more ordered carbon deposits. From the spectra in Fig. 8, the position of the G band (P_G) was also determined. This has also been related to the degree of graphitization of carbonaceous deposits: a higher P_G is related to greater order. P_G values were: 1588 cm^{-1} for $\text{CoIr}/\text{Ce}_{0.82}\text{Zr}_{0.18}900$ and $\text{CoIr}/\text{Ce}_{0.82}\text{Zr}_{0.18}700$ and 1584 cm^{-1} for $\text{CoIr}/\text{Ce}_{0.82}\text{Zr}_{0.18}500$ [36,37].

The TEM images of post-reaction catalysts (Fig. 9) also showed abundant carbon deposits over $\text{CoIr}/\text{Ce}_{0.82}\text{Zr}_{0.18}700$ and $\text{CoIr}/\text{Ce}_{0.82}\text{Zr}_{0.18}900$. From the results mentioned above, it was deduced that a higher calcination temperature of the support led to the formation of a more carbon deposits showing a higher degree of graphitization. Coke deposited on the metal surface during OSRB could partially be oxidized to CO_x by the oxide ions or hydroxyl groups coming from the support; and then the oxide or hydroxyl species on the surface would be recovered from O_2 or H_2O reactants. This process would result in a continuous coke-removal mechanism [38]. As stated above, in this work the calcination temperature of the support influenced the OSC of the catalyst; catalysts with lower OSC showed a lower capacity to activate water/oxygen [39].

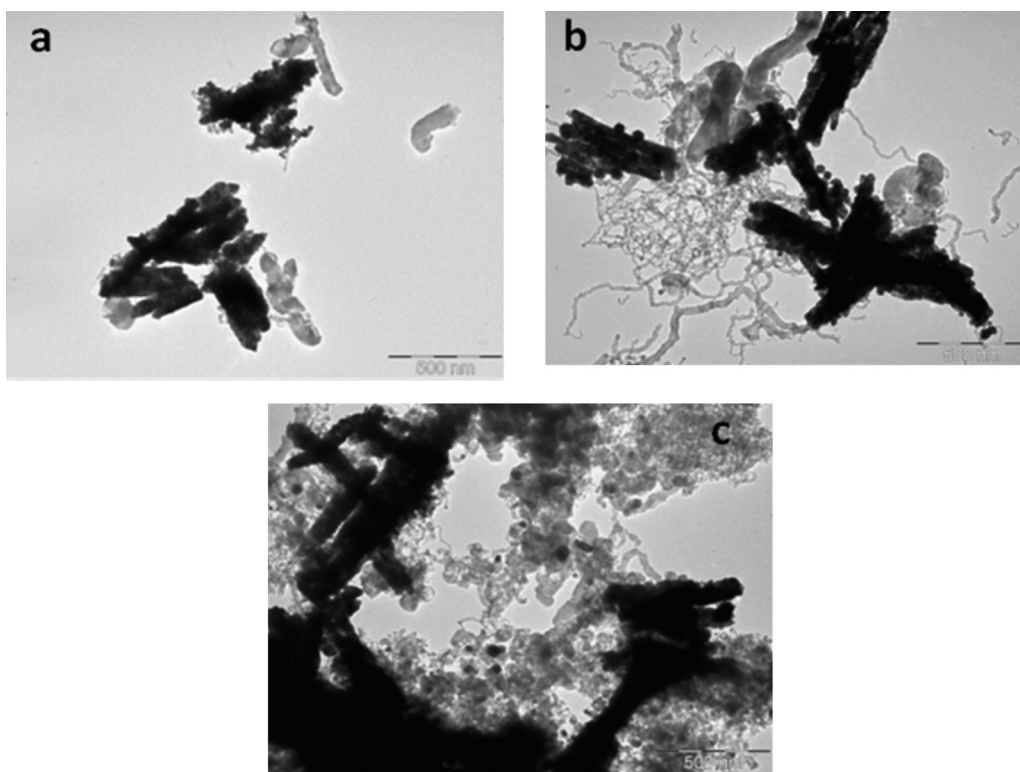


Fig. 9. TEM images of post-reaction catalysts. (a) CoIr/Ce_{0.82}Zr_{0.18}500; (b) CoIr/Ce_{0.82}Zr_{0.18}700; (c) CoIr/Ce_{0.82}Zr_{0.18}900.

4. Conclusions

The catalytic performance for OSRB of CoIr/Ce_{0.82}Zr_{0.18}O₂ catalysts depends on the characteristics of the support, which are determined by the calcination temperature of the CeZrO₂. An increase in the calcination temperature of the Ce_{0.82}Zr_{0.18}O₂ from 500 °C to 700 °C and 900 °C produced catalysts with a gradual increase in the crystallite size of the support, and a gradual lowering of both the degree of reduction of the support and the OSC. Moreover, the total number of basic sites decreased with the increase in the calcination temperature of the support from 500 °C to 700 °C and 900 °C. A calcination temperature of 700 °C or higher, produced the almost total disappearance of basic sites with moderate and strong strength. CoIr/Ce_{0.82}Zr_{0.18}500 showed the best catalytic performance in OSRB and it also showed the highest stability over time. CoIr/Ce_{0.82}Zr_{0.18}900 showed the highest deactivation over time and the greatest carbonaceous deposits; on this support, the water and/or oxygen activation at the metal-support interface which is necessary for carbon removal is not believed to be very efficient. However, the density of the structural defects in Ce_{0.82}Zr_{0.18}500, its OSC and its basicity characteristics are proposed to favour both oxygen diffusion from bulk to surface and the surface transfer of OH groups. These properties contribute to the oxidation of carbon deposits and maintain the catalyst stability.

Acknowledgements

The authors are grateful to Consolider Ingenio 2010-Multicat CSD2009-00050, MAT2011-23775, 2009SGR-0674 projects for financial support.

References

- [1] V.A. Goltsov, T.N. Veziroglu, L.F. Goltsova, *International Journal of Hydrogen Energy* 31 (2006) 153–159.
- [2] P. Ramírez de la Piscina, N. Homs, *Chemical Society Reviews* 37 (2008) 2459–2467.
- [3] D.B. Levin, R. Chahine, *International Journal of Hydrogen Energy* 35 (2010) 4962–4969.
- [4] C. Jin, M. Yao, H. Liu, C.F. Lee, J. Ji, *Renewable & Sustainable Energy Reviews* 15 (2011) 4080–4106.
- [5] W. Wang, Y. Cao, *International Journal of Hydrogen Energy* 35 (2010) 13280–13289.
- [6] G.A. Nahar, S.S. Madhani, *International Journal of Hydrogen Energy* 35 (2010) 98–109.
- [7] M.H. Youn, J.G. Seo, K.M. Cho, S. Park, D.R. Park, J.C. Jung, I.K. Song, *International Journal of Hydrogen Energy* 33 (2008) 1750–1753.
- [8] M. Araque, T.L.M. Martínez, J.C. Vargas, M.A. Centeno, A.C. Roger, *Applied Catalysis B: Environmental* 125 (2012) 556–566.
- [9] B.M. Reddy, A. Khan, Y. Yamada, T. Kobayashi, S. Lorient, J.C. Volta, *Langmuir* 19 (2003) 3025–3030.
- [10] G. Balducci, J. Kašpar, P. Fornasiero, M. Graziani, M.S. Islam, J.D. Gale, *Journal of Physical Chemistry B* 101 (1997) 1750–1753.
- [11] W. Cai, F. Wang, C. Daniel, A. van Veen, Y. Schuurman, C. Descorme, H. Provendier, W. Shen, C. Mirodatos, *Journal of Catalysis* 286 (2012) 137–152.
- [12] H.S. Roh, A. Platon, Y. Wang, D.L. King, *Catalysis Letters* 110 (2006) 1–6.
- [13] P. Biswas, D. Kunzru, *International Journal of Hydrogen Energy* 32 (2007) 969–980.
- [14] V. Dal Santo, A. Gallo, A. Naldoni, M. Guidotti, R. Psaro, *Catalysis Today* 197 (2012) 190–205.
- [15] W. Cai, P. Ramírez de la Piscina, N. Homs, *Bioresource Technology* 107 (2012) 482–486.
- [16] W. Cai, N. Homs, P. Ramírez de la Piscina, *Green Chemistry* 14 (2012) 1035–1043.
- [17] W. Cai, P. Ramírez de la Piscina, K. Gabrowska, N. Homs, *Bioresource Technology* 128 (2013) 467–471.
- [18] W. Cai, P. Ramírez de la Piscina, N. Homs, *Applied Catalysis B: Environmental* 145 (2014) 56–62.
- [19] E.B. Pereira, P. Ramírez de la Piscina, S. Martí, N. Homs, *Energy & Environmental Science* 3 (2010) 487–493.
- [20] E.B. Pereira, N. Homs, S. Martí, J.L.G. Fierro, P. Ramírez de la Piscina, *Journal of Catalysis* 257 (2008) 206–214.
- [21] F. Wang, W. Cai, H. Provendier, Y. Schuurman, C. Descorme, C. Mirodatos, W. Shen, *International Journal of Hydrogen Energy* 36 (2011) 13566–13574.
- [22] E. Mamontov, T. Egami, R. Brezny, M. Koranne, S. Tyagi, *Journal of Physical Chemistry B* 104 (2000) 11110–11116.
- [23] R. Kostic, S. Askrabic, Z. Dohcevic-Mitrovic, Z.V. Popovic, *Applied Physics A* 90 (2008) 679–683.
- [24] B.M. Reddy, G.K. Reddy, L. Katta, *Journal of Molecular Catalysis A: Chemical* 319 (2010) 52–57.

- [25] D.R. Sellick, A. Aranda, T. Garcia, J.M. López, B. Solsona, A.M. Mastral, D.J. Morgan, A.F. Carley, S.H. Taylor, *Applied Catalysis B: Environmental* 132–133 (2013) 98–106.
- [26] D.J. Kim, J.W. Jang, H.L. Lee, *Journal of the American Ceramic Society* 80 (1997) 1453–1461.
- [27] T. Yu, Y. Zhu, X. Xu, Z. Shen, P. Chen, C.T. Lim, J.T.L. Tong, C.H. Sow, *Advanced Materials* 17 (2005) 1595–1599.
- [28] D. Gallant, M. Pézolet, S. Simard, *Journal of Physical Chemistry B* 110 (2006) 6871–6880.
- [29] B. Jongsomjit, J. Panpranot, J.G. Goodwin Jr., *Journal of Catalysis* 215 (2003) 66–77.
- [30] E.I. Gürbüz, E.L. Kunkes, J.A. Dumesic, *Applied Catalysis B: Environmental* 94 (2010) 134–141.
- [31] I. Armelao, G. Bottaro, *Surface Science Spectroscopy* 10 (2003) 32–39.
- [32] N. Sheppard, T.T. Nguyen, in: R.J. Clark, R.E. Hester (Eds.), *Advances in Infrared and Raman Spectroscopy*, Wiley, New York, 1978.
- [33] N. Homs, A. Choplin, P. Ramírez de la Piscina, L. Huang, E. Garbowsky, R. Sánchez-Delgado, A. Théolier, J.M. Basset, *Inorganic Chemistry* 27 (1988) 4030–4033.
- [34] T. Nishiguhii, T. Matsumoto, H. Kanai, K. Utani, Y. Matsumura, W.J. Shen, S. Imamura, *Applied Catalysis A: General* 279 (2005) 273–277.
- [35] A.N. Fatsikostas, X.E. Verykios, *Journal of Catalysis* 225 (2004) 439–452.
- [36] P. Lespade, A. Marchand, M. Couzi, F. Cruege, *Carbon* 22 (1984) 375–385.
- [37] B. Valle, P. Castaño, M. Olazar, J. Bilbao, A.G. Gayubo, *Journal of Catalysis* 285 (2012) 304–314.
- [38] A.M. Silva, K. Regina de Souza, L.V. Mattos, G. Jacobs, B.H. Davis, F.B. Noronha, *Catalysis Today* 164 (2011) 234–239.
- [39] C. Descorme, Y. Madier, D. Duprez, *Journal of Catalysis* 196 (2000) 167–173.